International Journal of Heat and Mass Transfer 52 (2009) 2002–2008

Contents lists available at ScienceDirect

International Journal of Heat and Mass Transfer

journal homepage: www.elsevier.com/locate/ijhmt

Molecular dynamics simulation of thermal conductivity of nanocrystalline composite films

N.A. Roberts, D.G. Walker *, D.Y. Li

Department of Mechanical Engineering, Vanderbilt University, Nashville, TN 37235, USA

ARTICLE INFO

Article history:
Received 29 May 2008
Received in revised form 28 October 2008
Available online 30 December 2008

ABSTRACT

The efficiency of a thermoelectric material is measured by the figure of merit *ZT*, which is inversely proportional to the thermal conductivity. Superlattice structures often have a reduced thermal conductivity because of the introduction of interface scattering and, therefore, improved performance. The present work is focused on the effective thermal conductivity of nanocomposite films. This configuration could also improve *ZT* because of phonon-interface scattering introduced by the nanocrystals. The effects of crystal size and mass fraction are studied numerically using a molecular dynamics simulation. Results indicate that a reduction of 25% in the effective thermal conductivity can be achieved with the addition of nanocrystals which is comparable to that found in experimental measurement. However, the effective thermal conductivity was never reduced below the alloy limit.

1. Introduction

Nanostructured materials hold great promise for high-performance thermoelectric energy-conversion devices. Nanocrystalline composites (NCCs), which are bulk materials with embedded nanoparticles, may provide a favorable combination of effects that result in significant improvements in thermoelectric performance [1]. In particular, these materials show a decrease in thermal conductivity, which is inversely proportional to the thermoelectric figure of merit (*ZT*).

Two recent experiments, performed on a device similar to what is seen in Fig. 1, have shown that homogeneous host materials with embedded nanoparticles exhibit a decrease in thermal conductivity by a factor of 2 over that of the host material alone [2,3]. In these experiments a superlattice structure is created where the host layer is much thicker than a small epitaxial secondary layer. During an annealing step the thin layer forms a plane of uniformly distributed nanocrystals of uniform size. In the experiments the crystal size is systematically varied, and the thermal conductivity is measured. Presumably if the addition of nanocrystals does not alter the electrical conductivity or the Seebeck coefficient of the host material, then the thermoelectric performance will increase by a factor of 2 over that of the homogeneous material. These structures then become candidates for energy conversion devices. This performance is an improvement to that of previous efforts that used pure alloys to enhance thermoelectric energy conversion yielding values for $ZT \leqslant 1$ at room temperature [4].

Using molecular dynamics, the present work explores the mechanisms responsible for a reduced thermal conductivity of nanocrystalline composites compared to a homogeneous phase. In the limit of nanocrystals of zero size, the properties of the host are recovered. In the limit of large nanocrystals, the properties of the nanocrystalline material in bulk form are recovered. The thermal conductivity of both limiting cases is greater than that observed for the aligned nanocrystal case. Therefore, the reduction in thermal conductivity must be related to the structure and the crystal size.

From studies on superlattice structures by other researchers, we know that a reduction in thermal conductivity can be obtained over the properties of the constituent layers in a superlattice. The mechanisms for this reduction include interface scattering [5,6], and phonon phase interference introduced by the periodicity of the lattice, which creates phonon bands [7,8]. In 2000, Volz et al. observed a reduction in thermal conductivity with decreasing superlattice period (increasing interfacial area) in molecular dynamics simulations of Si/Ge superlattices [9]. In 2002, Daly et al. [10] also found a reduction in thermal conductivity with decreasing superlattice period using molecular dynamics. Molecular dynamics studies by Chen et al. [11,12] suggest that the reduction is largely diffuse scattering at the interface for lattice mismatched materials and that increased interfacial area results in a further reduced thermal conductivity. In 2006, Hegedus and Abramson performed molecular dynamics simulations of heterogeneous systems to study transport through interfaces between two dissimilar materials [13]. Stevens et al. also used molecular dynamics to study transport at solid–solid interfaces [14], and they found that the resistance to transport was largely governed by inelastic scattering for mismatched lattices. More recently Sun

* Corresponding author.
E-mail address: greg.walker@vanderbilt.edu (D.G. Walker).

0017-9310/$ - see front matter © 2008 Elsevier Ltd. All rights reserved.
doi:10.1016/j.ijheatmasstransfer.2008.10.027

Nomenclature

a	lattice constant (m)	T	temperature (K)
k	thermal conductivity (W/mK)	U	inter-atomic potential (J)
L	device length (m)	ZT	thermoelectric figure of merit
N	number of atoms	χ	size parameter
n	number fraction of krypton	ϵ	energy parameter (J)
R_i	interfacial thermal resistance	σ	lattice parameter (m)
R_m	material thermal resistance	ξ	crystal radius (m)
r	inter-atomic distance (m)		
r_{cut}	cutoff radius (m)		
S	Seebeck coefficient (μV/K)		

et al. [15] showed how different frequency phonons are involved in the transmission process across mismatched interfaces. All these studies tend to concur that for lattice matched materials, phonon interference dominates, and a minimum occurs for a period length comparable to the dominant phonon wavelength.

For nanocrystalline composites, the scattering mechanism is not likely a wave interference phenomenon because the interface between the matrix and the crystal is nonuniform. However, this complicated interface results in greater scattering due to a roughness associated with the interface. Furthermore, interference does not exist because the periodicity in [3] (10–40 nm) is much larger than the phonon wavelengths of the dominant heat-carrying phonons (1–3 nm) [16]. To reduce the effective thermal conductivity, the added particles must be particularly efficient scatterers. The size parameter, $\chi = 2\pi R/\lambda$, can provide an estimate of the wavelength involved in the particle-derived scattering processes, where λ is the phonon wavelength. Because the effective radius of the particles is of the same order as the dominant wavelengths, we are not likely in the Rayleigh regime. Consequently, the wavelengths that are scattered will be larger than the dominant phonon wavelength. This is important because the longer wavelength phonons have been shown to contribute most to the transport [15]. Compared to an alloy that scatters predominantly short wavelength phonons [3], this structure should provide an additional scattering mechanism that will ultimately reduce the thermal conductivity. Note that because our host is not an alloy, we are not predicting an overall reduction in conductivity compared to an alloy, but are identifying a reduction due to the nanocrystal alone.

This article presents a systematic numerical study of the effects of the size of nanoparticles on the effective conductivity of a nanocrystalline composite. The analysis involves a molecular dynamics study of a periodic array of crystals of varying sizes and atomic number fraction. In particular, we examine and explain the size-dependence of the thermal conductivity in NCCs and how these physical phenomena can be leveraged in nanostructured thermoelectric materials.

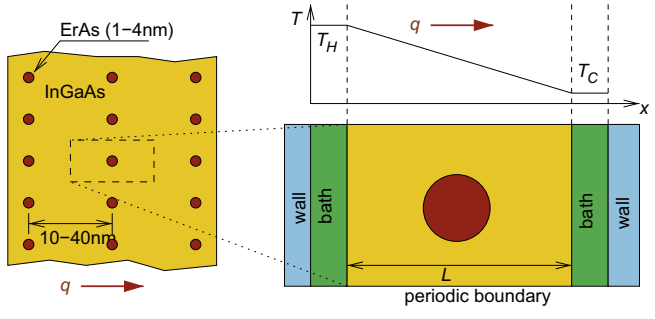

Fig. 1. Two-dimensional representation of a nanocrystalline composite superlattice with periods of 10–40 nm and nanorystals of 1–4 nm diameter (left). The structure mimics that of Ref. [3] where the host is InGaAs and the crystals are ErAs. Computational domain of this study (right) with applied temperatures of the baths (T_H = 60 K and T_C = 40 K). The walls contain fixed position atoms, and the top and bottom are periodic boundaries.

2. Analysis

The composite structure is composed of a matrix material (Ar) with embedded nanocrystals of a different material (Kr). Each component has a characteristic thermal conductivity, and we intend to study several combinations of these two materials to study how the structures alter phonon transport. The primary set of simulations involves a film of solid argon modeled with periodic boundary conditions in the infinite directions of the film (perpendicular to the direction of transport). In the center of the film, the atoms that fall within a spherical region are specified as krypton to simulate a nanocrystal embedded within the argon host (see Fig. 1). The radius of the sphere is systematically varied to explore the effect of the size of the crystal on thermal transport.

An FCC crystalline structure is assumed with a Lennard-Jones inter-atomic potential given as

$$U = 4\epsilon\left[\left(\frac{\sigma}{r}\right)^{12} - \left(\frac{\sigma}{r}\right)^{6}\right]. \quad (1)$$

The structures contain two materials whose property values are given in Table 1. For materials above 20% of the Debye temperature, which for argon θ_D = 85 K, the thermal conductivity is largely dominated by scattering induced by the anharmonicity of the inter-atomic potential [17]. This effect will govern the effective thermal conductivity of a homogeneous argon film. As also suggested in Ref. [14] other potentials should be explored. By including a second material with different lattice constant and different stiffness, a scattering interface has been introduced that should decrease the thermal conductivity over the bulk case.

Table 1
Parameters used for the different materials in the simulations [11]. For potentials between different atoms, the energy parameter $\epsilon_{12} = \sqrt{\epsilon_1\epsilon_2}$ and the length parameter $\sigma_{12} = (\sigma_1 + \sigma_2)/2$.

Material	Parameter	Value
Kr	ϵ (J)	2.25×10^{-21}
	σ(m)	3.65×10^{-10}
	a (m)	5.69×10^{-10}
	m (kg)	1.39×10^{-25}
	r_{cut} (m)	9.49×10^{-10}
Ar	ϵ (J)	1.67×10^{-21}
	σ (m)	3.4×10^{-10}
	a (m)	5.3×10^{-10}
	m (kg)	6.63×10^{-26}
	r_{cut} (m)	8.84×10^{-10}

A time step size of 1 fs for 400,000 time steps, where the data are recorded after 20,000 time steps to reach a quasi-steady state, provide a good sampling time for averaging [18]. The uncertainty is estimated by calculating the standard deviation of energy added at each bath for 100,000 time steps. This value is divided by the total energy added (for each bath) to obtain a percent fluctuation in the heat flux of 4.2–5.2% for all cases. The time step and length of the simulation (0.4 ns) were obtained from the thermal relaxation time of argon which is approximately 10 ps. The size of the films used for these simulations varied from $8 \times 8 \times 8$ UC to $16 \times 16 \times 16$ UC with an additional 10 UC (5 on each side) in the direction of transport for the wall and bath where UC is the FCC unit cell. In the wall and bath regions, 4 UC (2 on each side) were used as fixed position walls as shown in Fig. 1. This strategy was used to prevent evaporation from the non-periodic boundaries. The bath temperatures are held constant at 40 and 60 K for the cold and hot sides, respectively, by maintaining a constant average kinetic energy for each bath so that a non-equilibrium simulation could be performed. The approach and configuration have been used successfully by other researchers [18]. The entire structure is composed of no fewer than 4608 atoms (for $8 \times 8 \times 8$ UC) where 2560 are wall and bath atoms and a maximum of 26,624 atoms (for $16 \times 16 \times 16$ UC). The simulation was started at an initial temperature of 50 K.

The effective thermal conductivity is calculated from Fourier's law for steady conduction,

$$q = -kA\frac{\Delta T}{L}, \tag{2}$$

where L is the length of the structure between the two constant bath layers. Fourier's law is a phenomenological law where the thermal conductivity is considered a proportionality constant or "effective" property. Similar simulations in the literature add a fixed amount of energy to each bath at each time step and the temperatures are calculated [19]. In our case we can calculate the energy required to maintain a fixed temperature at each bath. This energy divided by the time step is the heat transfer rate q in Eq. (2). Using kinetic arguments, the bath temperature in terms of the atomic velocities is

$$\frac{3}{2}Nk_B T = \sum_i^N \frac{1}{2}m_i v_i^2, \tag{3}$$

where N is the number of atoms in the bath. As such, the temperature difference in Eq. (2) is fixed, and the heat transfer is averaged over long times [18] to establish a stable value. Using this approach, we observe that the average temperature per plane is fairly linear through the structure, where the temperature is calculated from the kinetic energy of each plane (see Fig. 2) suggesting that Fourier's law is not a bad approximation.

In a thick film where the device is much larger than the mean free path of phonons, the interface scattering could be considered negligible. In such a case, an equivalent resistance circuit can be developed to describe the effective conductivity of the composite

$$k_{\text{eff}} = (1-n)k_{\text{Ar}} + nk_{\text{Kr}}, \tag{4}$$

where multi-dimensional conduction is reduced to a number fraction weighted average of the two bulk conductivities with n being the number fraction of krypton. This expression is analogous to a bulk expression for a binary system in series. We chose a series system as opposed to a parallel system because the crystal approximately divides the domain into series components. In addition, a parallel analysis does not change the results significantly. Fig. 3 shows the effective conductivity of the composite material if interface scattering is ignored. For a crystal radius of zero, there is no krypton and the conductivity is that of the argon. As the crystal radius increases, the krypton, which has a higher conductivity, contributes to the effective conductivity of the composite. The largest the radius can become is 1/2 the film width. At this point, the crystal fills the space such that adjacent crystals in the periodic domain are connected. However, the conductivity of the krypton is not recovered because even in this limiting case, some argon still exists in the corners not occupied by the spherical particle. Notice that because this model does not allow interface resistance, the conductivity of our NCC system is nowhere less than the conductivity of either bulk material unlike experimental observations.

Because the continuum model (Eq. (4)) does not match observations for highly scaled devices, we must add an additional interface resistance R_i so that the effective conductivity of the nanocomposite can be approximated as

$$k_{\text{eff}} = \left[\frac{1-n}{k_{\text{Ar}}} + \frac{n}{k_{\text{Kr}}} + \frac{A}{L}R_i\right]^{-1}, \tag{5}$$

where A is the cross-sectional area perpendicular to the direction of transport, and L is the thickness of the film. For an embedded crystal the maximum number of krypton atoms occurs when the crystal radius is equal to half the width of the simulation domain w, such that $n_{\max} = \pi w/6L$.

Presumably the interface resistance R_i is dependent on the orientation of interfaces that contribute to the total interfacial area.

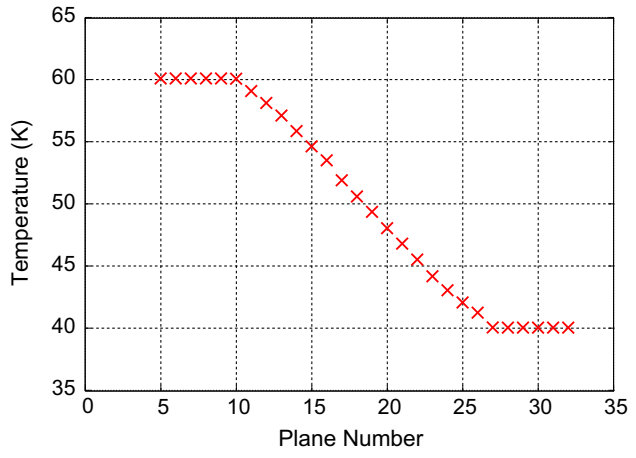

Fig. 2. Temperature distribution for an $8 \times 8 \times 8$ UC simulation device with $\xi = 3$ UC.

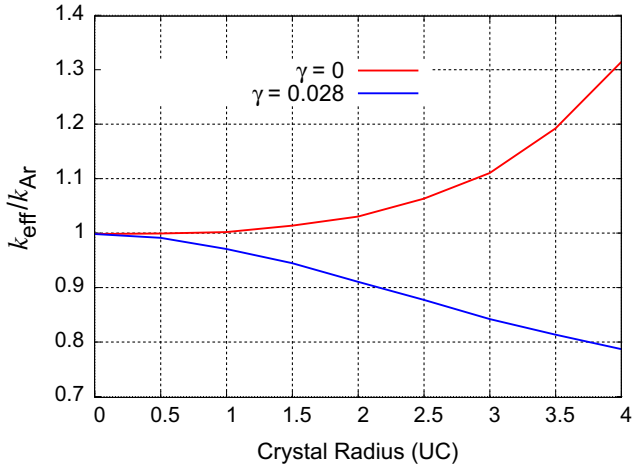

Fig. 3. Simple analytic fitting model given by Eq. (4) (top curve) and Eq. (5) (bottom curve).

As results will show, the contribution to the reduction of thermal conductivity is different for interfaces normal and parallel and is dominated by interfaces normal to the direction of transport. Because scattering at diffuse interfaces is isotropic, the difference between parallel and normal interfaces suggests that phonon interference is a significant factor. Nevertheless, good agreement can be obtained by considering scattering at interfaces normal to the direction of transport only. Consequently, we will use only the normal or projected interfacial area in the analytic model and an expression for R_i will be obtained from the molecular dynamics studies.

3. Results

Fig. 4 shows the conductivity of an argon film of various thicknesses and with no embedded crystal. Not only can we predict the bulk conductivity of argon, which agrees well with measurements, but also this plot illustrates the size effects associated with scaled systems. Because the computational domain is small, the simulations included herein do not contain the full complement of phonon frequencies found in a bulk system and therefore, the conductivity is already reduced compared to bulk systems. However, we are interested in reductions derived from the inclusion of a nanocrystal, which follow from the remainder of the simulations.

Results of the molecular dynamics study for various crystal sizes are shown in Fig. 5. As the crystal increases in size, we might expect the thermal conductivity to increase because we are essentially replacing a low conductivity material (Ar) with a large conductivity material (Kr). However, the figure shows that the conductivity decreases with an increase in crystal size, which is presumably governed by the increase in interface area between the crystal and the host material. This artifact supports the hypothesis that the conductivity is dominated by interface scattering. The solid lines in this figure represent the simplified model and show reasonable agreement with the molecular dynamics data. The analytic model in Eq. (5), however, does not consider phonon interference effects and multi-dimensional transport explicitly. Instead because interface scattering presumably dominates, these secondary effects are wrapped into the interface scattering resistance, which is a fitting parameter. The validity of this assumption will be explored. The three cases in Fig. 5 represent different film thicknesses. In all cases the lattice is periodic in the infinite directions every 8 UC. Therefore, the largest crystal radius is 4 UC. The

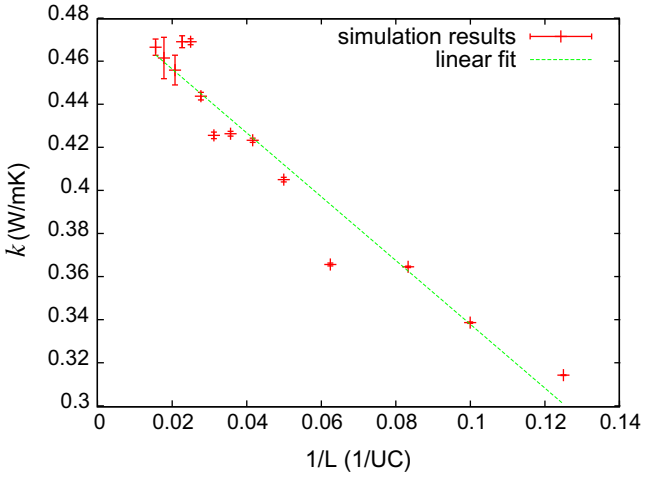

Fig. 4. Conductivity of films of argon for varying thicknesses. Extrapolation of the linear fit to zero (infinite thickness) represents the bulk argon value.

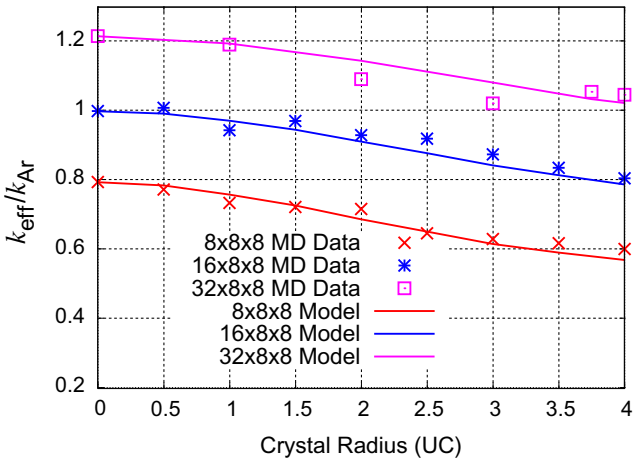

Fig. 5. Dimensionless thermal conductivity as a function of the nanocrystal radius. The interface model is Eq. (5) for $R_i = 0.028$ K/UC^2 W.

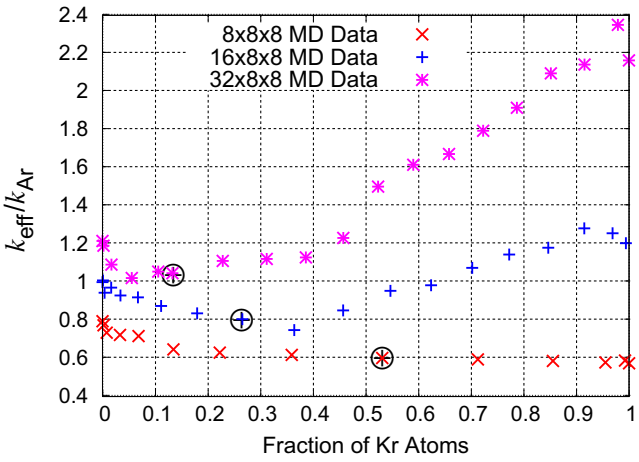

Fig. 6. Dimensionless thermal conductivity as a function of the nanocrystal number of krypton atoms. Circles indicate inscribed sphere, number fractions greater than these points represent increasing the amount of krypton with a spherical interface between Ar and Kr.

difference in the magnitude of the conductivity between the three cases arises from the addition of longer wavelength phonons to the simulation (see Fig. 4). To account for this feature in the analytic model the bulk conductivities k_{Ar} and k_{Kr} in Eq. (2) are derived from a simulation of the same length for homogeneous materials (no embedded crystals) at the nominal (and arbitrary) length of 16 UC. A marked reduction in conductivity is seen as the projected area of the crystal increases.

The same molecular dynamics data from Fig. 5 is shown in Fig. 6 as a function of the fraction of krypton atoms (n). For the region beyond the largest crystal (inscribed sphere denoted by the circle) the conductivity increases approximately linearly. As the crystal radius is increased, the projected area normal to the transport direction does not increase substantially since the area can only be as big as the cross-section of the structure. Instead the increase is due primarily to the increase in fraction of krypton atoms n, which increases nearly linear with crystal radius. Consequently, the conductivity increases linearly with n as in Eq. (5).

To better understand the origin of the decrease in k we will now look at some alternate simulations which are designed to isolate individual effects on the thermal conductivity.

First consider simulations in which the material ratio is held constant at 50% while the interfacial area is varied to avoid the

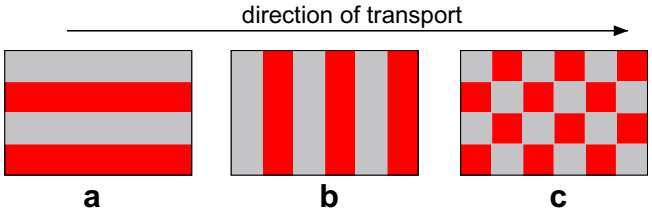

Fig. 7. Schematic of constant atomic ratio simulations. (a) Parallel superlattice. (b) Normal superlattice. (c) 3-D checkerboard.

confounding effect of varying mass fraction. To investigate the impact of different types of interfaces (normal and parallel to transport) we present three different systems which include normal and parallel interface superlattice structures and a system that includes both types of interfaces where the structure is a periodic array of alternating material cubes in all three directions (3-D checkerboard pattern), which form blocks. A schematic of these are shown in Fig. 7. In each of these systems the interfacial area was varied by changing the period length (layer thickness or block size) from 1 up to 32 UC. Fig. 8 shows the results of the conductivity of the device as a function of the block size. The area available for phonon scattering is estimated as the area of a single block face times the number of blocks times 6 sides per block divided by 2. By varying the block size we can increase the area for scattering. Because the block simulations have more interface area, we see a marked decrease in conductivity compared to the crystal case. In the long domain case (64 UC), a minimum in the conductivity occurs at a block size of 2 UC. This observation is a consequence of the long-range order of the device. As the block size is reduced, it is possible that phonon band gaps are produced because of the difference between the short and long-range orders of the structure, which has been observed previously in molecular dynamics simulations [20]. In essence the blocks create a basis for additional acoustic modes. This causes a change in the frequency components that can contribute to the overall transport. If the block size continues to decrease, the short-range order of the devices contributes very little to the overall transport by limiting the phonon wavelengths while the long wavelengths become more abundant, which increases transport. When this occurs there is no longer a phonon band gap, and thermal conductivity increases, which is what we see as we move from a block size of 2–1 UC. This increase in conductivity as the block size is decreased below 2 UC does not appear in the shorter devices because of the absence of the additional long

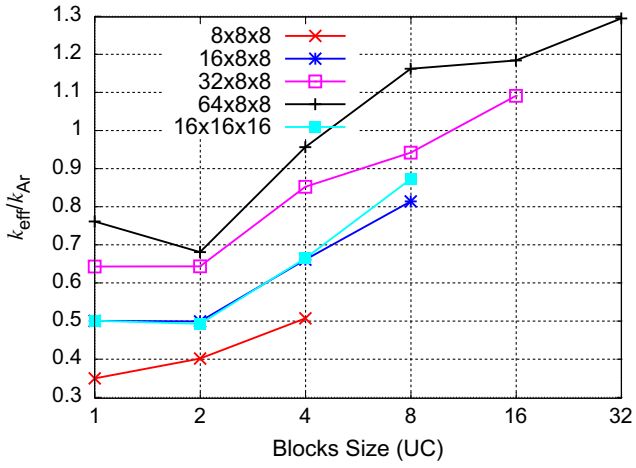

Fig. 8. Thermal conductivity of blocks as a function of the block size.

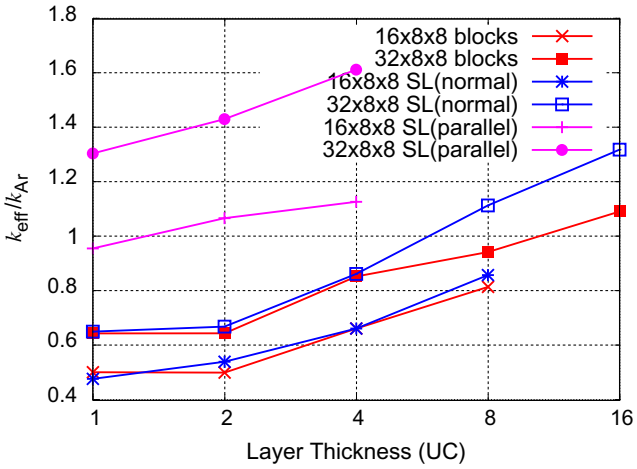

Fig. 9. Comparison between blocks and superlattice with interfaces normal and parallel to the direction of transport as a function of the period of the structures.

wavelength phonons. This is also why the longer devices have increased thermal conductivity due to the existence of longer wavelength phonons that can contribute to transport. These results also agree with those found by Lukes et al. [18] where an increase in the cross-section of the domain (greater than 4×4 UC) made no discernible difference in thermal conductivity and those predicted by several groups where superlattice layers produced phonon band gaps that reduced thermal conductivity when the layer thicknesses were of the order of or below the average phonon mean free path [8,12,21,10]. Fig. 9 shows the thermal conductivity of the normal and parallel superlattice structures as well as the block structure as a function of the layer thickness or block size. The normal and parallel superlattices are similar to the block simulations except the parallel superlattices do not include any interfaces normal to the direction of transport and the normal superlattices do not include any interfaces parallel to the direction of transport. The area of the parallel superlattice structure is 2/3 that of the blocks, and the normal superlattice structure is 1/3 that of the blocks. If normal and parallel interfaces have the same impact on thermal conductivity we should see a comparable change in the thermal conductivity, but this does not occur. Fig. 9 shows that the block and normal superlattice structures result in nearly equivalent reduction in the thermal conductivity while the parallel superlattice results in a greater thermal conductivity. The reason for the difference in thermal conductivity between the block and normal superlattice structures and the small reduction in the parallel superlattice is unclear. As suggested earlier, diffuse scattering effects are isotropic and the direction of the interface should not affect the results. Therefore, these results suggest that the reduction may be related to confinement in the directions normal and perpendicular to the direction of transport. Nevertheless, the analytic model, which considers scattering the dominant mechanism, results in a error of less than 10%.

A simulation involving a single planer interface was used to investigate the thermal conductivity as a function of the atomic number fraction only. In this case the interfacial area was minimized and remained constant at 128 UC^2 while the number fraction was varied by changing the location of the interface along the direction of transport. Since the interfacial area is not changing our model predicts an increase in the thermal conductivity from that of argon to that of krypton. Fig. 10 shows the results as a function of the atomic fraction of krypton in the device. These results show good agreement with the analytic model with a interface resistance of $R_i = 0.029$ K/UC^2 W. This value of R_i is slightly different that the one used for the single crystal case where $R_i = 0.028$ K/

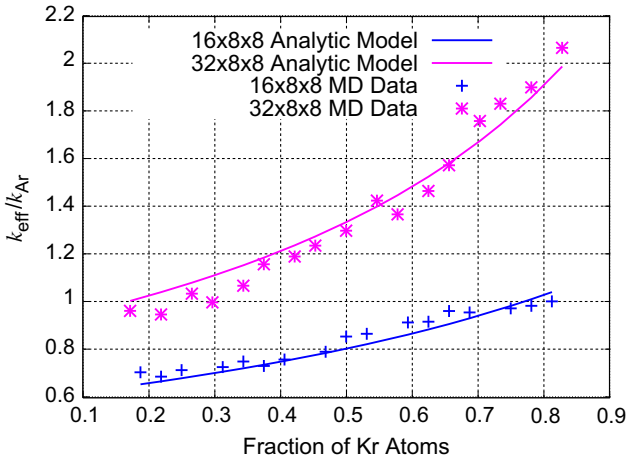

Fig. 10. Results from a single interface as a function of the number fraction of krypton atoms.

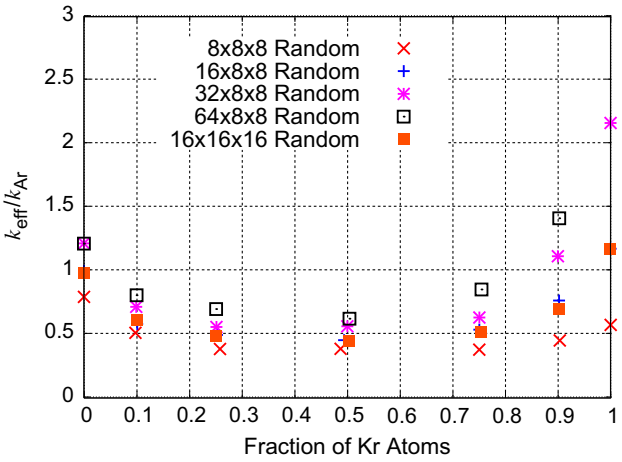

Fig. 12. Dimensionless thermal conductivity as a function of the number of krypton atoms. The interface model is Eq. (5).

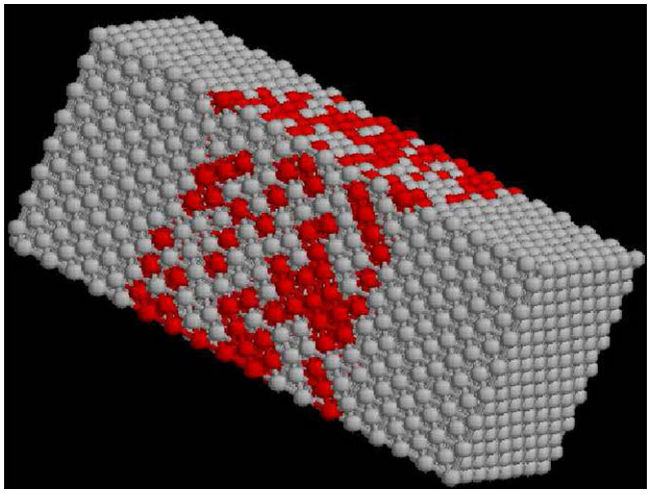

Fig. 11. Example of the random distribution at 50% fraction of krypton atoms. The fraction of krypton was varied to produce the results in Fig. 12.

UC^2 W, because the type of interfaces present are different, the parallel interfaces in the crystal do contribute some to the overall thermal conductivity reduction.

Finally, we consider a device that is composed of randomly distributed atoms where the fraction of krypton is varied. This case was of interest because it can approximate an alloy (see Fig. 11), which scatters short wavelength phonons efficiently. Much work has been done that shows the thermal conductivity can be reduced with low-dimensional structures, but reduction below the alloy limit has been a topic of great interest. Kim et al. [3] presented results of a reduction below the alloy limit by a factor of 2, though the reduction was the result of embedding a nanoparticle of a different material. Cahill et al. [22] presented experimental evidence showing that superlattices of Si–Ge (5 nm [23] and 4.4 nm period [24]) and GaAs–AlAs (5.67 nm period [5]) resulted in thermal conductivities lower than that of the respective alloys [23,25], though the difference was relatively small. The results from these simulations are shown in Fig. 12 which identify a minimum in the thermal conductivity when the device is composed of 50% krypton. One could argue that the interfacial area in an alloy is actually quite large compared to the other cases, which results in a large reduction in the thermal conductivity. In fact the random simulation is 37% smaller than the best crystal case and resulted in the greatest reduction in conductivity of all the configurations studied, only slightly lower than the normal superlattice and block simulations.

4. Conclusions

The thermal conductivity of nanocrystalline composite films was examined using molecular dynamics. The primary intent was to determine the mechanisms by which nanocrystals reduce thermal conductivity. To do this, several structures were examined to isolate the roles of interfaces, both parallel and normal to the direction of transport. As expected, the dominant mechanism appeared to be the interfacial area, specifically those normal to the direction of transport. Our results show that increased interfacial area created by the presence of the nanocrystal reduces the effective thermal conductivity of the film. Although this effect is believed to be the result of an increase in interfacial area, secondary effects such as phonon confinement or limits on the frequency content, also contribute to the observed reduction. From the various structures and the molecular dynamics data obtained from the single embedded nanocrystal, a simple analytic model was developed. This bulk-like model includes the thermal conductivities of each of the constituent materials along with a resistance due to the interface (R_i). Although we are using a bulk model we have found reasonable agreement in the prediction of the thermal conductivity of a nanocrystalline composite. It is also interesting to note that the effect of the interfacial resistance in the single interface ($R_i = 0.029$ K/UC^2 W) and the embedded nanocrystal ($R_i = 0.028$ K/UC^2 W) were very close. The difference in the direction of the interfaces accounts for this difference. Although these results provide a qualitative understanding of the influence of interfacial area in NCC's, the magnitude of the effect cannot be estimated for other materials in the foregoing work.

In this work we did not find a reduction in thermal conductivity resulting from embedded nanocrystals down to the alloy limit. We did, however, find reductions in the thermal conductivity of the same order as those found experimentally for a periodic array of embedded nanocrystals (25% reduction in thermal conductivity from the host material) showing that embedded nanocrystals are capable of reducing thermal conductivity. The minimum alloy thermal conductivity in our study was determined from the random case, which resulted in a reduction greater than a factor of 2. We also found large reductions in the block and normal superlattice cases where we had large amounts of interfacial area. These results showed, when compared to a superlattice, that the

interfaces perpendicular to the direction of transport contributed to the reduction much more than those parallel. Based on these findings, maximum interfacial area perpendicular to transport is needed to achieve a large reduction in the thermal conductivity. With the addition of a single nanocrystal we are limited with the amount of interfacial area we can achieve in the system. The results imply that embedding multiple nanocrystals along the direction of transport could result in larger reductions in the thermal conductivity from an increased interfacial area.

References

[1] H.L. Ni, X.B. Zhao, T.J. Zhu, X.H. Ji, J.P. Tu, Synthesis and thermoelectric properties of Bi_2Te_3-based nanocomposites, J. Alloys Compd. 397 (1–2) (2005) 317–321.

[2] T.C. Harman, P.J. Taylor, M.P. Walsh, B.E. La Forge, Quantum dot superlattice thermoelectric materials and devices, Science 297 (27) (2002) 2229–2232.

[3] W. Kim, J. Zide, A. Gossard, D. Klenov, S. Stemmer, A. Shakouri, A. Majumdar, Thermal conductivity reduction and thermoelectric figure of merit increase by embedding nanoparticles in crystalline semiconductors, Phys. Rev. Lett. 96 (045901) (2006).

[4] R.F. Service, Semiconductor advance may help reclaim energy from 'lost' heat, Science 311 (5769) (2006) 1860.

[5] W.S. Capinski, H.J. Maris, T. Ruf, M. Cardona, K. Ploog, D.S. Katzer, Thermal-conductivity measurements of GaAs/AlAs superlattices using a picosecond optical pump-and-probe technique, Phys. Rev. B 59 (12) (1999) 8105–8113.

[6] Scott T. Huxtable, Alexis R. Abramson, Chang-Lin Tien, Arun Majumdar, Chris LaBounty, Xiaofeng Fan, Gehong Zeng, John E. Bowers, Ali Shakouri, Thermal condictivity of Si/SiGe and SiGe/SiGe superlattices, Appl. Phys. Lett. 80 (10) (2002) 1339–1737.

[7] R. Venkatasubramanian, Lattice thermal conductivity reduction and phonon localization-like behavior in superlattice structures, Phys. Rev. B 61 (4) (2000) 3091–3097.

[8] M.V. Simkin, G.D. Mahan, Minimum thermal conductivity of superlattices, Phys. Rev. Lett. 84 (5) (2000) 927–930.

[9] S. Volz, J. Saulnier, G. Chen, P. Beauchamp, Computation for thermal conductivity of Si/Ge superlattices by molecular dynamics techniques, Microelectron. J. 31 (2000) 815–819.

[10] B. Daly, H. Maris, K. Imamura, S. Tamura, Molecular dynamics calculation of the thermal conductivity of superlattices, Phys. Rev. B (2002).

[11] Y.F. Chen, D.Y. Li, J.K. Yang, Y.H. Yu, J.R. Lukes, A. Majumdar, Molecular dynamics study of the lattice thermal conductivity of Kr/Ar superlattice nanowires, Physica B 349 (1–4) (2004) 270–280.

[12] Y. Chen, D. Li, J.R. Lukes, Z. Ni, M. Chen, Minumum superlattice thermal conductivity from molecular dynamics, Phys. Rev. B 72 (174302) (2005) 1–6.

[13] P.J. Hegedus, A.R. Abramson, A molecular dynamics study of interfacial thermal transport in heterogeneous systems, Int. J. Heat Mass Transfer 49 (2006) 4921–4931.

[14] R.J. Stevens, L.V. Zhigilei, P.M. Norris, Effects of temperature and disorder on thermal boundary conductance at solid–solid interfaces: non-equilibrium molecular dynamics simulations, Int. J. Heat Mass Transfer 50 (2007) 3977–3989.

[15] L. Sun, J.Y. Murthy, Molecular dynamics simulation of phonon scattering at rough semiconductor interfaces, in: ITherm, Orlando, Florida, May 2008, pp. 1078–1086.

[16] W. Kim, R. Wang, A. Majumdar, Nanostructuring expands thermal limits, Nanotoday 2 (1) (2007) 40–47.

[17] H. Kaburaki, J. Li, S. Yip, Thermal conductivity of solid argon by classical molecular dynamics, Mater. Res. Soc. Symp. Proc. (1999).

[18] J.R. Lukes, D. Li, X.-G. Liang, C.-L. Tien, Molecular dynamics study of solid thin-film thermal conductivity, J. Heat Transfer 122 (3) (2000) 536–543.

[19] T. Ikeshoji, Bjorn Hafskjold, Non-equilibrium molecular dynamics calculation of heat conduction in liquid and liquid–gas interface, Mol. Phys. 81 (2) (1994) 251–261.

[20] A.J.H. McGaughey, M.I. Hussein, E.S. Landy, M. Kaviany, G.M. Hulbert, Phonon band structure and thermal transport correlation in a layered diatomic crystal, Phys. Rev. B 74 (2006).

[21] G. Chen, Phonon wave heat conduction in thin films and superlattices, J. Heat Transfer 121 (1999) 945–953.

[22] D.G. Cahill, K.E. Goodson, A. Majumdar, Thermometry and thermal transport in micro/nanoscale solid-state devices and structures, J. Heat Transfer 124 (2002) 223–241.

[23] S.M. Lee, D.G. Cahill, R. Venkatasubramanian, Thermal conductivity of Si–Ge superlattices, Appl. Phys. Lett. (1997).

[24] T. Borca-Tasciuc, W.L. Liu, J.L. Liu, T.F. Zeng, D.W. Song, C.D. Moore, G. Chen, K.L. Wang, M.S. Goorsky, T. Radetic, R. Gronsky, T. Koga, M.S. Dresselhaus, Thermal conductivity of symmetrically strained Si/Ge superlattices, Superlattice Microstruct. (2000).

[25] M.A. Afromowitz, Thermal conductivity of GaAlAs alloys, J. Appl. Phys. 44 (1973) 1292–1294.